Journal of Pathology
J Pathol December 2024; **264:** 434–447
Published online 25 October 2024 in Wiley Online Library
(wileyonlinelibrary.com) DOI: 10.1002/path.6358

ORIGINAL ARTICLE

A comprehensive luminal breast cancer patient-derived xenografts (PDX) library to capture tumor heterogeneity and explore the mechanisms of resistance to CDK4/6 inhibitors

Ilenia Segatto[1*†], Maria Chiara Mattevi[1†], Gian Luca Rampioni Vinciguerra[1,2], Nicole Crestan[1], Lorena Musco[1], Andrea Favero[1], Alessandra Dall'Acqua[1], Gabriele Di Giustino[1], Giorgia Mungo[1], Sara D'Andrea[1], Chiara Gava[1], Federica Ruggiero[1], Matteo Dugo[3], Lorenzo Gerratana[4], Fabio Puglisi[4], Samuele Massarut[5], Riccardo Bomben[6], Maurizio Callari[7], Tiziana Perin[8], Gustavo Baldassarre[1] and Barbara Belletti[1*]

[1] *Unit of Molecular Oncology, Centro di Riferimento Oncologico di Aviano (CRO), IRCCS, National Cancer Institute, Aviano, Italy*
[2] *Faculty of Medicine and Psychology, Department of Clinical and Molecular Medicine, University of Rome 'Sapienza', Santo Andrea Hospital, Rome, Italy*
[3] *San Raffaele Hospital, Milan, Italy*
[4] *Department of Medical Oncology, Centro di Riferimento Oncologico di Aviano (CRO), IRCCS, National Cancer Institute, Aviano, Italy*
[5] *Unit of Breast Surgery, Centro di Riferimento Oncologico di Aviano (CRO), IRCCS, National Cancer Institute, Aviano, Italy*
[6] *Unit of Clinical and Experimental Onco-Hematology, Centro di Riferimento Oncologico di Aviano (CRO), IRCCS, National Cancer Institute, Aviano, Italy*
[7] *Fondazione Michelangelo, Milan, Italy*
[8] *Unit of Pathology, Centro di Riferimento Oncologico di Aviano (CRO), IRCCS, National Cancer Institute, Aviano, Italy*

**Correspondence to: B Belletti or I Segatto, Unit of Molecular Oncology, Centro di Riferimento Oncologico di Aviano (CRO), IRCCS, National Cancer Institute, Via F. Gallini, 2, 33081 Aviano, Italy. E-mail: bbelletti@cro.it (B Belletti) or isegatto@cro.it (I Segatto)*

[†]These authors contributed equally to this work.

Abstract

Breast cancer (BC) is marked by significant genetic, morphological and clinical heterogeneity. To capture this heterogeneity and unravel the molecular mechanisms driving tumor progression and drug resistance, we established a comprehensive patient-derived xenograft (PDX) biobank, focusing particularly on luminal (estrogen receptor, ER+) and young premenopausal patients, for whom PDX models are currently scarce. Across all BC subtypes, our efforts resulted in an overall success rate of 17% (26 established PDX lines out of 151 total attempts), specifically 15% in luminal, 12% in human epidermal growth factor receptor 2 positive (HER2+) and 35% in triple negative BC. These PDX mirrored morphologic and genetic features of BC from which they originated, serving as a reliable tool to investigate drug resistance and test therapeutic strategies. We focused on understanding resistance to CDK4/6 inhibitors (CDK4/6i), which are crucial in the treatment of patients with advanced luminal BC. Treating a sensitive luminal BC PDX with the CDK4/6i palbociclib revealed that, despite initial tumor shrinkage, some tumors might eventually regrow under drug treatment. RNA sequencing, followed by gene set enrichment analyses, unveiled that these PDXs have become refractory to CDK4/6i, both at biological and molecular levels, displaying significant enrichment in proliferation pathways, such as *MTORC1*, *E2F* and *MYC*. Using organoids derived from these PDX (PDxO), we observed that acquisition of CDK4/6i resistance conferred cross-resistance to endocrine therapy and that targeting MTORC1 was a successful strategy to overcome CDK4/6i resistance. Considered together, these results indicate that our PDX models may serve as robust tools to elucidate the molecular basis of BC disease progression and, by providing the possibility to simultaneously test different therapies on the same tumor, to surmount treatment resistance. While this approach is of course not feasible in the clinic, its exploitation in PDX may expedite the identification and development of more successful therapies for patients with advanced luminal BC.

Keywords: patient-derived xenograft; breast cancer; luminal breast cancer; estrogen receptor positive breast cancer; tumor heterogeneity; CDK4/6 inhibitor; drug resistance; endocrine therapy; tumor organoid; MTORC1

Received 8 May 2024; Revised 7 August 2024; Accepted 4 September 2024

No conflicts of interest were declared.

Introduction

Breast cancer (BC) is characterized by a high degree of heterogeneity, manifesting at both intra-tumoral and inter-tumoral levels. Different BC subtypes display different grades of biological complexity and unique behaviors in terms of incidence, survival, pattern of metastasis and response to therapies. In clinical practice, a simplified categorization based on hormone receptor (HR) status (estrogen receptor, ER, and progesterone receptor,

PR) and human epidermal growth factor receptor 2 (HER2) expression is commonly used to distinguish the luminal (HR+, HER2−), the HER2 positive (either luminal, HR+ and HER2+, or basal, HR− and HER2+) and the triple negative (TN, HR− and HER2−) BC subgroups [1–5]. However, to meet the scope of precision oncology, BC heterogeneity urgently needs to be taken into account, underscoring the necessity for preclinical models that faithfully recapitulate individual tumors, with their own biological complexity and variability in treatment responses.

From this point of view, patient-derived xenografts (PDXs), generated by implantation and serial transplantation of human tumors into immune-deficient mice, hold great promise as a discovery platform to develop more effective cancer therapies. PDXs not only closely mirror human tumors from which they originate at histological and molecular levels, but also exhibit high concordance in treatment responses and metastatic dissemination [6–8]. For all these reasons, PDXs are rapidly supplanting traditional cell lines and xenografts as preferred models for conducting translational research. However, their use is limited by some factors, such as high cost and, not last, the finite number of models available.

Although a growing number of BC PDXs have been globally established during the last decade, there are still significantly underrepresented tumors in the collections reported so far. Luminal breast cancer (LBC), by far the most common subtype in Western populations (approximately 70% of all BC cases), is further subclassified into luminal A (high ER expression, low grade and Ki67 proliferation index) and luminal B (high/low ER expression, higher grade and Ki67 proliferation index), with distinct clinical outcomes [2,9,10]. Together with the HER2+ subtype, LBC (especially luminal A) are less represented in existing PDX collections.

LBCs typically respond to endocrine therapies, which act by depleting estrogen production or interrupting ER signaling. However, many factors can contribute to the emerrgence of endocrine therapy resistance, eventually leading to tumor recurrence or progression. Combining CDK4/6 inhibitors (CDK4/6i) with endocrine therapy has proven clinically effective and represents now the first-line treatment for patients with advanced LBC [11,12]. However, resistance to CDK4/6i almost invariably arises in these patients, emphasizing the critical need to comprehend these mechanisms and develop new strategies to overcome resistance [13–15].

Here, we report on the generation and characterization of a panel of 26 BC PDXs, strategically designed to address urgent medical research needs. Our efforts focused on enhancing representation of luminal BC subtype (both A and B), from which PDXs are the most challenging to develop, as well as incorporating samples from young patients and resistant to endocrine therapy and/or chemotherapy. As a tool to study tumor evolution under the pressure of therapy, we have generated and characterized PDX models displaying *de novo* or acquired resistance to CDK4/6i. Our results demonstrate that these models may actually serve as a discovery platform and to test novel, tailored and more successful therapeutic approaches, to advance preclinical research to precision oncology.

Materials and methods

Ethical approval and breast cancer tissue collection

Human specimens were collected from patients with BC undergoing surgery in our Institute (BCRO samples), upon signing an informed consent form. The research was permitted by the Institutional Review Board of CRO Aviano (IRB-06-2017) and complied with all relevant ethical regulations, including the Declaration of Helsinki. BC specimens were collected in a non-consecutive manner based on tissue availability, possibility to process and specific interest in the clinicopathological features of each tumor. In brief, following surgical resection and pathological evaluation, the tumor fragments dedicated to this protocol were rapidly transferred in ice to the research laboratory. Here, working within a tissue culture hood (class II), after the removal of fat and/or healthy tissue, the tumor was cut into 3–4 mm cubes and stored in RPMI-1640 (Gibco, Waltham, MA, USA) supplemented with 10% fetal bovine serum (FBS, Gibco) on ice until implantation (within a few hours of surgery). If the implantation was postponed to the following day, tumor fragments were stored at 4°C for up 24 h in Tissue Storage Solution (MACS®, Miltenyi Biotec, Bergisch Gladbach, Germany). Other tumor fragments, when available, were stored in freezing medium (10% dimethyl sulfoxide, DMSO) for future utilization.

Animal experimentation

Animal experimentation was approved by the Italian Ministry of Health and our Institutional Animal Care and Use Committee (OPBA) (authorizations 616/2015-PR, 838/2020-PR and 342/2023-PR). All *in vivo* experiments were conducted strictly following internationally accepted guidelines for animal research (FELASA, https://felasa.eu/working-groups/guidelines/id/14, 2012). Mice were housed in the animal facility of CRO Aviano under controlled environmental parameters (22°C with 40–60% humidity), pathogen free cabinets and following a 12 h dark/light cycle. Mice were monitored at least twice a week for the entire duration of the project and euthanized by injection of excess anesthetic.

PDX establishment, propagation and characterization using immunohistochemistry (IHC)

PDXs were generated following the protocol published in 2013 by Alana Welm and colleagues [16], using 3–4 week old female immune-compromised NOD/SCID/IL2Rγ−/− (NSG) mice (Charles River Laboratories, Wilmington, MA, USA), implanted with fresh or freshly thawed tumor fragments in the cleared inguinal mammary fat pad, bilaterally. Both human breast tumor and

PDX tissues were fixed in 4% paraformaldehyde, embedded in paraffin wax and analyzed using H&E and automated IHC staining (Ultraview Detection Kit cat. #760-500; Ventana, Roche, Basel, Switzerland). HER2 status was measured and reported according to ASCO-CAP 2018 guidelines [17], then breast tumors were classified in accordance with WHO 2019 [18]. Detailed protocols are presented in Supplementary materials and methods.

Generation of palbociclib-resistant LBC PDX, PDxO and 3D-survival analysis

Stable third-passage PDX derived from luminal BCRO#28 and BCRO#18 were implanted in NSG mice (10 mice/PDX) and continuously treated via oral gavage with vehicle or palbociclib (PD-0332991 hydrochloride, Clinisciences, Nanterre, France). Organoids were generated from fresh PDX tumors, processed as described in [19] and plated in 3D-matrix drops for survival assays (CellTiter-Glo® 3D Cell Viability Assay, Promega, Madison, WI, USA). Detailed protocols are presented in Supplementary materials and methods.

DNA and RNA purification, NGS and RT-qPCR analyses

The Maxwell® 16 Tissue DNA Purification Kit (Promega, Madison, WI, USA) was used for automated purification of DNA from fresh solid tumor samples, following the manufacturer's instructions. Total RNA was isolated from fresh solid tumor samples using TRIzol solution (Invitrogen, Thermo Fisher Scientific, Waltham, MA, USA), following the manufacturer's protocol and as described previously [20]. An input of 25 ng of DNA was used for subsequent mutational analysis by next-generation sequencing (NGS). *PIK3CA*, *AKT1* and *TP53* mutational status was investigated by NGS with an amplicon-based strategy, as described previously [21,22]. RNA-Seq libraries were generated using the Illumina Stranded total RNA prep library kit (Illumina, San Diego, CA, USA) following the protocol's instructions. RNA from tumor samples was extracted as described above. RNA was reverse transcribed using a 5× PrimeScript RT Master Mix (Takara Bio, Kusatsu, Japan). Reverse transcriptase-quantitative polymerase chain reaction (RT-qPCR) analyses were performed essentially as described [23,24]. Detailed protocols are presented in Supplementary materials and methods.

Bioinformatic analyses

Somatic mutation calling

PIK3CA, *AKT1* and *TP53* somatic mutations were analyzed as described previously [21]. Single nucleotide variants of possible clinical significance were evaluated by curated analyses using the Catalogue of Somatic Mutations in Cancer (COSMIC, https://cancer.sanger.ac.uk/cosmic) and International Cancer Genome Consortium (ICGC, https://dcc.icgc.org/) data portals. NGS data were mapped to the human reference genome (GRCh37/hg19, https://www.ncbi.nlm.nih.gov/assembly/GCF_000001405.13) and analyzed using VariantStudio™ (Illumina) and Integrative Genomics Viewer softwares and annotated. Only somatic alterations called at allele frequencies ≥1% and that were confirmed in at least two distinct runs were considered mutated. Synonymous variants and polymorphisms described in the Single Nucleotide Polymorphism Database (dbSNP138) were removed. Results were expressed as a percentage of variant allele frequency.

RNA sequencing data processing

Quality control of FASTQ files was performed using the FastQC tool (https://www.bioinformatics.babraham.ac.uk/projects/fastqc/). To distinguish between human and mouse reads we applied the In silico Combined human-mouse Reference Genome approach [25]. In brief, we created an *in silico* reference genome by combining GRCh38 Homo sapiens and GRCm39 Mus musculus reference genomes. Related gene annotations were obtained from Gencode v42 and Gencode v31 for human and mouse, respectively. Then, reads were aligned using STAR v2.5.2 [26] against the merged genome. Finally, raw read counts were obtained for human and mouse genes according to the – quantMode option of STAR set to GeneCounts.

Differential gene expression and gene set enrichment analyses were performed as described in Supplementary materials and methods.

Statistical analyses

Data are presented as mean ± SD or box plots with the median values indicated, as specified in each figure legend. Statistically significant differences were determined using Student's or Mann–Whitney tests, as appropriate. p values of less than 0.05 were considered statistically significant. Data analysis was performed using GraphPad Prism 8 (GraphPad Inc., San Diego, CA, USA).

Results

Generation of a living biobank of breast cancer samples and patient-derived xenografts

High-quality biospecimens are critical for preserving tissue vitality and for their successful utilization, such as tumor implantation in mice and/or organoids generation. We thus established a collaboration with the Pathology Unit and implemented a robust pipeline for the collection of fresh BC specimens. In this way, the time between surgery and sample processing, for direct implantation, storing or freezing, was held below 2 h. Specimens of BC were collected from consenting patients at our Institute, in a non-consecutive manner, based on tissue availability, possibility to process and interest in the clinicopathological features of the tumor.

The vast majority of tumor specimens were obtained from patients with early stage, operable BC at the time of surgery. We particularly, but not exclusively, focused on the ER+, HER2− BC (hereafter luminal, i.e. LBC) subtype, which represents the most common BC subtype (60–70% of all BC), with a specific attention for LBC arising in young premenopausal women, overall focusing on tumors for which the availability of PDX models is scarcer than for other subtypes [6]. However, we also established some HER2+ BC (both ER+ HER2+, i.e. HER2 luminal; and ER− HER2+, i.e. HER2 basal) and triple negative BC (ER− HER2−, i.e. TN). For PDX establishment and propagation, we used NSG mice and followed the protocol published in 2013 by Derose *et al* [16]. To maximize engraftment and growth of LBC, which is challenging due to the relatively slow growth rate and the dependence on estrogen, we established and maintained all LBC PDX lines with subcutaneous hormone pellets.

It is known that not all tumors successfully engraft in mice and a bias for aggressive phenotypes is commonly observed. However, thanks to our pipeline, we were able to observe good engraftment rates with all BC subtypes, even with primary samples of LBC known in the literature to be the most difficult to engraft, often reported as 0%, especially with luminal A samples [6,27–29]. Our statistics ranged from 22% of luminal A (LBC with Ki67 < 20%), 33% of luminal B (LBC with Ki67 > 20%) to 60% of HER2 basal samples. Altogether, we attempted the implantation of 151 BC samples and obtained 44 successful first engraftments, with an overall initial take rate of 29% (Table 1).

A PDX was deemed as 'established' when it had been passed through three consecutive passages in NSG mice. Our final take rate diminished a bit (especially in luminal A samples) but remained aligned with the engraftment rate, in the different BC subtypes, showing a clear advantage only in the TN subtype: 15/103 LBC (15%), of which 5/49 luminal A (10%) and 10/54 luminal B (18%); 3/25 HER2+ (12%), of which 2/20 luminal (10%) and 1/5 basal (20%); and 8/23 TN (35%) (Table 1). Consistent with the take rate, the time intercurrent between implantation of the surgical sample and the appearance of a sizeable tumor that could be passed into a second generation of mice was highly different between specimens and quite consistent within subtypes. The TN was the most rapid (median time to engraft from implantation = 21 weeks), while the luminal A specimens were the slowest (median time to engraft from implantation = 46 weeks) (Figure 1A,B).

We then looked at clinicopathological features of the 26 BC specimens that we successfully established (Table 2) and all 151 that were attempted (supplementary material, Tables S1 and S2). Altogether, we implanted 126 primary tumors, 14 recurrences and 11 metastatic (lymph node) samples, all invasive ductal carcinomas. In contrast to other reports, we observed that success of engraftment was similar among primary tumors (17.5%, 22/126); local recurrences (14.3%, 2/14); and lymph node metastases (18.2%, 2/11) [6].

Engraftment success correlates with tumor grade and noPCR after neo-adjuvant treatment, but not with age or mutation in *PIK3CA* or *TP53*

As mentioned, our collection was non-consecutive, driven by specific interest in LBC and enriched for young patients. We thus wondered if age, as a surrogate marker of aggressiveness, could represent a predictive factor for the take rate in PDX. We considered the tumors from patients who were pre-menopausal (Y, ≤45 years of age) and post-menopausal (*n*Y, ≥55 years of age) and excluded those who were peri-menopausal (46–54 years of age). We obtained stable BC PDX in 18/118 from Y (15%) and 4/20 from *n*Y (20%).

Next, we compared samples collected from patients after neo-adjuvant treatment who did not reach pathological complete response (PCR), with all the others, which were treatment naïve. We observed that among post-neo-adjuvant samples, 9/17 engrafted (52.3%), while 17/134 engrafted (12.7%) among treatment naïve samples, altogether indicating that not reaching a PCR was a strong indicator for take rate. The same was true for tumor grade, confirming that this variable significantly affected take rate, with no G1 sample successfully engrafted (0/2), 10% success for G2 (5/51) and 23% for G3 (21/92) samples (6, grade unknown).

Surprisingly, mutations in the two most commonly mutated genes in BC, *PIK3CA* and *TP53* (supplementary material, Table S3) also did not have an impact on the engraftment success. The take rate was 13% for *PIK3CA* mutated (8/63) and 21% for *PIK3CA* wild type (18/87) BC; 17.2% for *TP53* mutated (11/64) and 17.4% for

Table 1. Take rate, number and percentage of early passage and established patient-derived xenografts (PDXs), divided by breast cancer (BC) subtype.

BC subtype	PDX take rate			Established	% of take rate from literature
	I engraftment	II passage	III passage		[6,27–29]
Luminal A	11/49 (22%)	7/49 (14%)	6/49 (12%)	5/49 (10%)	0–15%
Luminal B	18/54 (33%)	10/54 (18%)	10/54 (18%)	10/54 (18%)	
HER2 luminal	3/20 (15%)	3/20 (15%)	2/20 (10%)	2/20 (10%)	11–40%
HER2 basal	3/5 (60%)	1/5 (20%)	1/5 (20%)	1/5 (20%)	
Triple negative	9/23 (39%)	8/23 (35%)	8/23 (35%)	8/23 (35%)	17–60%
All	44/151 (29%)	29/151 (19%)	27/151 (18%)	26/151 (17%)	

Abbreviation: HER2, human epidermal growth factor receptor 2.

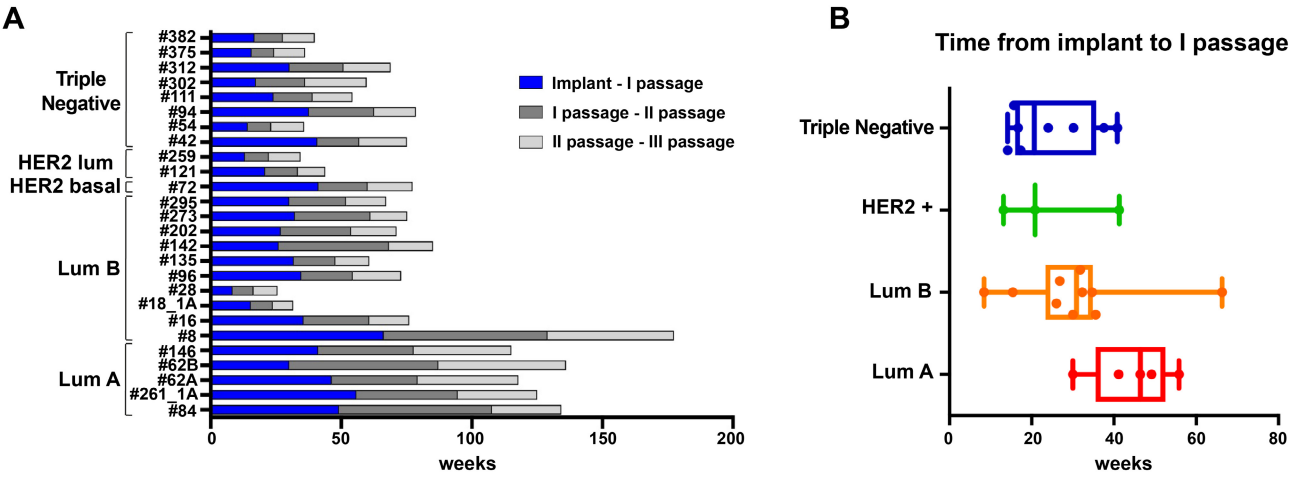

Figure 1. Take rate and time to engraftment in patient-derived xenografts (PDXs) from different breast cancer subtypes. (A and B) For each established PDX, grouped for subtype, graph shows time (in weeks) taken to obtain a stable model. In blue, bars show the weeks from the implant of the surgical sample to the collection of xenografts at first passage; in dark grey, from implant of first passage tumor to collection of second passage xenografts; in light grey, from implant of second passage tumors to collection of third passage xenografts. HER2, human epidermal growth factor receptor 2; Lum, luminal.

TP53 wild type (15/86) (one sample unknown), suggesting that the ability to engraft and survive in this initially hostile environment may be independent of these gene alterations. Of note, while *TP53* alterations were always maintained (with similar or increased variant allele frequency, VAF), *PIK3CA* sub-clonal mutations (i.e. below 5% of VAF) present in the original tumor were often lost in the derived PDX. One interesting exception was

Table 2. Clinico-pathological features of patients with breast cancer (BC) for whom patient-derived xenografts (PDXs) were established ($n = 26$).

Clinico-pathological features	BC subtype			
	Luminal ($n = 15$)	HER2 luminal ($n = 2$)	HER2 basal ($n = 1$)	Triple negative ($n = 8$)
Age (years)				
Median	42	66.5	40	44.5
Range	29–57	43–90	-	32–86
Engrafted sample				
Primary tumor	14 (93.3%)	1 (50%)	0	7 (87.5%)
Lymph metastasis	0	1 (50%)	1 (100%)	1 (12.5%)
Local recurrence	1 (6.7%)	0	0	0
Pathological type				
IDC	15 (100%)	2 (100%)	1 (100%)	8 (100%)
ILC	0	0	0	0
Tumor grade				
G1	0	0	0	0
G2	4 (26.7%)	0	0	1 (12.5%)
G3	11 (73.3%)	2 (100%)	1 (100%)	7 (87.5%)
Tumor stage				
I	5 (33.3%)	0	0	4 (50%)
II	7 (46.7%)	1 (50%)	0	3 (37.5%)
III	3 (20%)	1 (50%)	0	1 (12.5%)
IV	0	0	1 (100%)	0
		0		
Nodal status				
N0	7 (46.7%)	1 (50%)	0	7 (87.5%)
N+	8 (53.3%)	1 (50%)	1 (100%)	1 (12.5%)
				0
Pre-treatment				
Yes	6 (40%)	0	0	3 (37.5%)
No	9 (60%)	2 (100%)	1 (100%)	5 (62.5%)
Tumor take	15/103 (14.5%)	2/20 (10%)	1/5 (20%)	8/23 (34.8%)

Note: Data are numbers (%) unless specified otherwise. IDC, invasive ductal carcinoma; ILC, invasive lobular carcinoma.

PDX#312 that showed the appearance of a clonal *PIK3CA* E542K mutation (VAF 43.1%) not observed in the original BCRO#312 tumor (supplementary material, Table S3).

Characterization of PDXs

To study the tumor features of the established xenografts, we performed pathological analyses on the 26 established PDX lines, comparing them to corresponding tumors. In all cases, the morphological and architectural characteristics of the patient's tumor were reproduced in the PDX, whatever the histopathological type (supplementary material, Figures S1–S3). ER, PR and HER2 expression (or lack of) were reproducible, with small fluctuations, in all xenografts (supplementary material, Figures S1, S2 and Table S2). In line with previous reports, we generally observed a higher expression of HER2 in PDX compared with the corresponding tumor and a lower expression of ER and PR in luminal tumors. As reported by others [8,30], the proliferation index, assessed by IHC for Ki67, showed a trend toward higher mitotic activity in all PDX compared with their corresponding patient's tumor (supplementary material, Table S2).

Generation of CDK4/6i resistant PDX

For patients with advanced LBC, first-line treatment is currently represented by endocrine therapy (tamoxifen, fulvestrant or aromatase inhibitors) combined with a CDK4/6 inhibitor (CDK4/6i), such as palbociclib (palbo). Although CDK4/6i have been quite successful in this setting, not all patients respond, and occurrence of resistance is frequent and invariably associated with disease progression. However, studies of the biological features linked to CDK4/6i resistance are limited by the lack of adequate preclinical models. With the aim of generating such models, we selected PDX from two patients with LBC (BCRO#18 and BCRO#28) who, according to their pathological features, could in principle be candidates for treatment with CDK4/6i, in case of disease progression. BCRO#18 was obtained from a 31 year-old woman subjected to neo-adjuvant treatment, while BCRO#28 was from a treatment naïve 57 year-old patient. Once established in mice, both tumors maintained similar characteristics to their corresponding ones in patients, except for an increase in Ki67 in both PDX#18 and PDX#28 and a decrease in PR in PDX#28 (supplementary material, Figure S2). To verify CDK4/6i sensitivity, we treated mice carrying 50–100 mm^3 tumors with daily oral gavage of palbo (100 mg/kg, 5 days/week), monitoring tumor growth over time (Figure 2A). PDX#18 displayed a primary (or intrinsic) resistance to palbo and, after only 3 weeks, tumors reached the critical mass endpoint, in both treated and untreated groups (Figure 2B). On the other end, PDX#28 tumors became highly sensitive to palbo and immediately started to shrink and almost disappeared (untreated sensitive US; treated sensitive, TS; Figure 2C). However, by keeping mice under palbo treatment for over 6 months, two mice developed a secondary (or acquired) resistance and tumors started to regrow (treated resistant, first round, TR1) (Figure 2C, at late time points). To confirm that these tumors had become stably palbo-resistant, we re-implanted the two TR1 tumors into a new generation of NSG mice (second round, R2). When tumors became 50–100 mm^3, mice were randomized to remain untreated (vehicle, UR2) or treated with daily palbo, as in the first round (TR2) (Figure 2A). UR2 and TR2 tumors grew at the same rate, either when untreated or treated with palbo, indicating that they maintained the palbo-resistance (Figure 2D).

Characterization of palbociclib resistance

Next, we analyzed tumors from both rounds to evaluate possible changes in tumor biomarkers and gene expression between palbo-sensitive and palbo-resistant tumors. During the first round, palbo-treated tumors collected when they were still sensitive to the drug (TS) displayed very low expression of Ki67 and pRB compared with their untreated sensitive counterpart (US), in line with the expected anti-proliferative response to CDK4/6i (Figure 3A–E). However, looking at resistant tumors from the first (TR1) and second round, either treated or untreated (UR2 and TR2), they all displayed high levels of Ki67 and pRB, in line with the acquisition of a resistant phenotype (Figure 3A–E). All tumors maintained similar morpho-pathological features; however, all resistant tumors displayed a quite significant decrease in PR expression (Figure 3A–E), possibly indicating a more aggressive and endocrine insensitive behavior, as observed in patients with LBC.

We next looked at the development of metastatic lesions. In the palbo-sensitive group, 3/3 untreated mice developed lung metastases, but palbo treatment completely abolished their formation (0/6 mice) (Figure 3F). Notably, when tumors emerged from palbo prolonged treatment (TR1) were re-implanted in the second round, lung metastases formed at a considerably higher rate than in the first round, and at a similar level between the treated and untreated mice (Figure 3F). These results indicated that, under the pressure of prolonged palbo treatment, a more invasive population was selected and that palbo was now completely ineffective in restraining the metastatic spreading of these tumors.

To better investigate the molecular mechanisms that could underlie the acquisition of CDK4/6i resistance, we performed whole transcriptome RNA sequencing of tumor samples from both sensitive and resistant tumors. Gene enrichment analyses clearly showed no significant gene enriched in the TR versus UR comparison, demonstrating that these tumors were essentially insensitive to the presence of the drug, while significantly enriched transcripts were present either when TR were compared with TS or when UR were compared with US (Figure 4A), as also confirmed by RT-qPCR analysis in some representative genes from TR versus UR comparison (supplementary material, Figure S4). A heatmap of significant gene set enrichment analysis showed that pathways related to proliferation were effectively shut down

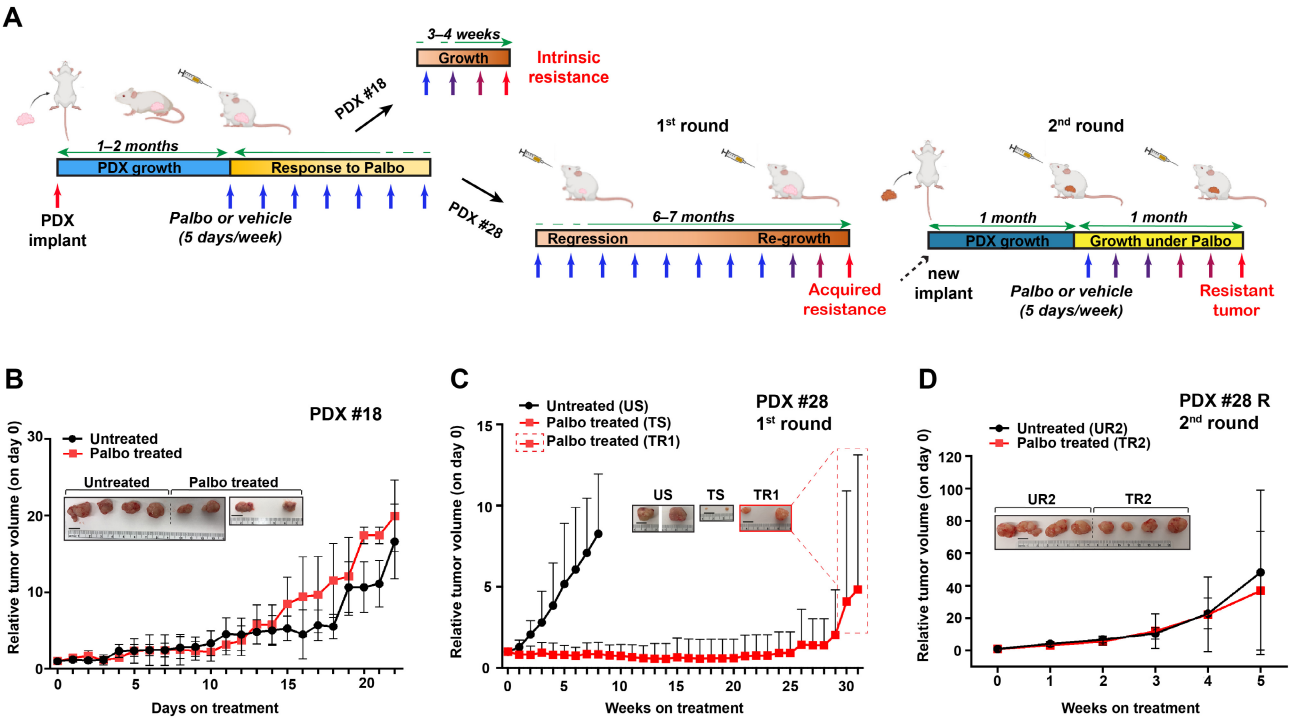

Figure 2. Generation of patient-derived xenografts (PDXs) resistant to CDK4/6 inhibitor palbociclib. (A) Schematic overview of the experimental workflow used to induce the acquisition of resistance to the CDK4/6 inhibitor palbociclib. Two different stable luminal PDXs (PDX#18 and PDX#28) were implanted in NSG mice and, when tumor volume reached about 60 mm^3, mice were treated with vehicle or palbociclib (palbo, 100 mg/kg, oral gavage, 5 days/week) and the tumor volume was weekly monitored. PDX#18 displayed intrinsic resistance to palbo, continued to grow, and 3–4 weeks from the first treatment mice were sacrificed (upper part). PDX#28 were sensitive to palbo: under treatment, tumors started to regress, but after 6–7 months of continuous exposure to palbo, some tumors started to regrow and acquired resistance to the drug (lower part, first round). These resistant tumors were collected, implanted in a new cohort of mice and treated again with vehicle or palbo (lower part, second round). Tumors continued to grow in presence of the drug, confirming the acquisition of a resistant phenotype. Created in part with BioRender.com. (B) Graph shows tumor growth of PDX#18, treated or not with oral palbociclib, as described in (A). Inset displays some representative tumors collected from untreated or palbo-treated mice. Scale bar, 1 cm. (C) Graph shows tumor growth of PDX#28, treated or not with oral palbociclib, as described in (A) (first round). Red dashed box indicates tumor regrowth following a prolonged exposure to palbo. Inset displays some representative images of untreated sensitive (US), palbo-treated sensitive (TS) and palbo-treated resistant (TR1) tumors. Scale bar, 1 cm. (D) Graph shows tumor growth of palbo-resistant tumors (TR1) emerging from first round in (C) and treated with vehicle (UR2) or palbociclib (TR2) for a second round, as described in (A). Inset displays some representative images of untreated resistant (UR2) and palbo-treated resistant (TR2) tumors. Scale bar, 1 cm. In each graph, tumor volume is plotted as its size at the time of first treatment (day 0). Mean ± SD.

by palbo treatment in sensitive tumors (TS versus US) but were reverted in resistant ones (TR versus TS and UR versus US) (Figure 4B and supplementary material, Figure S5A). No clear difference in these pathways was observed comparing TR with UR, confirming at the molecular level that treatment with palbo of these resistant tumors did no longer elicit any cell cycle restrictive effect (Figure 4B). These findings were confirmed looking at the NES plots of three of the most significant pathways related to proliferation, *MYC*, *E2F* and *MTORC1*, showing a significant enrichment in all comparisons between sensitive and resistant tumors (TR versus TS and UR versus US) (Figure 4C). In accord, S6 ribosomal protein, a downstream target of the MTORC1 pathway, was hyperactivated in both untreated and treated resistant tumors compared with sensitive ones, as measured by immunohistochemical staining of phospho-Ser 240/244 sites (Figure 4D). Under palbo, pathways related to the induction of inflammatory and immune responses were upregulated in tumor cells even after the resistant phenotype was acquired (Figure 4B, TR versus UR, upper part of the heatmap), although much less than in sensitive tumors (TR versus TS).

Next, we looked at the stromal counterpart, detected by data alignment to the murine transcriptome. Here, we not only observed the upregulation of pro-proliferative pathways, in synchro with what was seen in the tumor cells counterpart, but also an intriguing enrichment of extracellular matrix remodeling and epithelial-mesenchymal transition pathways, especially in resistant versus sensitive tumors under treatment (TR versus TS) (Figure 5A,B and supplementary material, Figure S5B). These modifications of the stromal microenvironment are possibly involved in the acquisition of the resistant phenotype, either by promoting or by facilitating tumor cell survival in the presence of palbociclib.

Inhibition of the MTORC1 pathway overcomes CDK4/6i resistance

Upregulation of the MTORC1 pathway during acquisition of CDK4/6i resistance is consistent with data

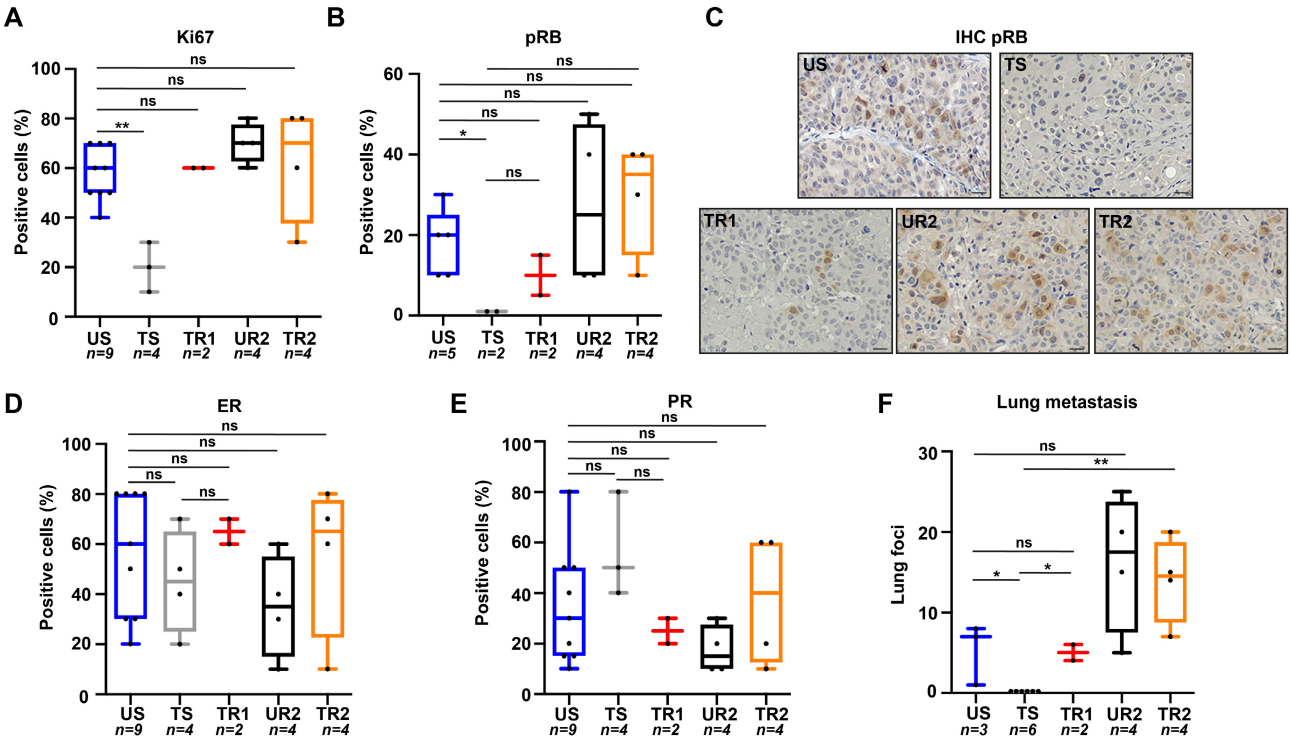

Figure 3. Palbociclib resistant tumors show increased proliferative features. (A and B) Box plots report the percentage of cells positive for Ki67 proliferation marker (A) or retinoblastoma protein phosphorylated on serine 780 (pRB) (B), performed by immunohistochemistry (IHC) on PDX#28 tumor sections from mouse cohorts described in Figure 2A. (C) Representative IHC images of pRb in the indicated groups, acquired using 20× objective. Scale bar, 100 μm. (D and E) Box plots show the percentage of cells positive for estrogen receptor (ER) (D) or progesterone receptor (PR) (E), as described in (A). (F) Graph reports the number of metastatic foci detected in pan-cytokeratin-stained sections of lungs, collected from the same mice described in (A). In all graphs, the number of individual tumors analyzed is reported under each box. Statistical significance calculated using Mann–Whitney test and expressed by p value <0.05. *$p < 0.05$; **$p < 0.01$, ns, not significant. US, untreated sensitive; TS, treated sensitive; TR1, treated resistant, first round; UR2, untreated resistant, second round; TR2, treated resistant, second round.

already reported in the literature [31–33]. Further, many MTORC1 inhibitors are already available in clinic for the treatment of patients with advanced LBC [34], thus providing a promising and feasible way to overcome CDK4/6i resistance. To test this possibility in the context of patient-derived models, sticking as much as possible to real world scenarios, we generated cultures of PDX-derived organoids (PDxO) from both palbo-sensitive and palbo-resistant tumors (PDxO-Sens/Res). First, we validated that PDxO-Res maintained their palbo-sensitivity/resistance in culture. Significantly higher survival of PDxO from resistant PDX tumors was evident both at 5 μM and at 15 μM concentrations, respectively, able to kill approximately 50% and 100% of PDxO-Sens (Figure 6A,B). Interestingly, using endocrine therapies commonly used in clinic to treat patients with LBC, such as tamoxifen and fulvestrant, we observed that palbo-resistance in PDxO-Res conferred cross-resistance to both these drugs (Figure 6C). Next, we tested whether the addition of the MTORC1 inhibitor rapamycin was able to restore sensitivity to CDK4/6i in PDxO-Res. First, while PDxO-sens were very sensitive to rapamycin, PDxO-Res were quite resistant to it, in line with the fact that this pathway was hyperactivated in palbo-resistant PDX (Figure 4B–D). However, when we used the combination of palbo and rapamycin, while the PDxO-Sens did not display significant differences compared with each treatment alone, the PDxO-Res became much more sensitive to this combination (Figure 6D). These results suggest that the hyperactivation of the MTORC1 pathway may represent an essential step during the acquisition of the resistant phenotype and, at the same time, a synthetic lethal target specific for these resistant tumors. Therefore, our finding has unveiled a druggable vulnerability that may have an immediate translatability in clinic to overcome palbo-resistance in patients with BC.

Discussion

In BC, tumor heterogeneity is closely tied to therapeutic resistance and poor patient outcome. Exploring this heterogeneity and developing novel and more effective anticancer agents require robust preclinical models that are able to recapitulate the complexity and the course of human BC disease. Unfortunately, most traditional BC models do not meet these criteria.

To address this challenge, we, on one side, set up an optimized protocol for tumor biobanking, since it represents an essential part of any cancer research project. In parallel, we have established a comprehensive living

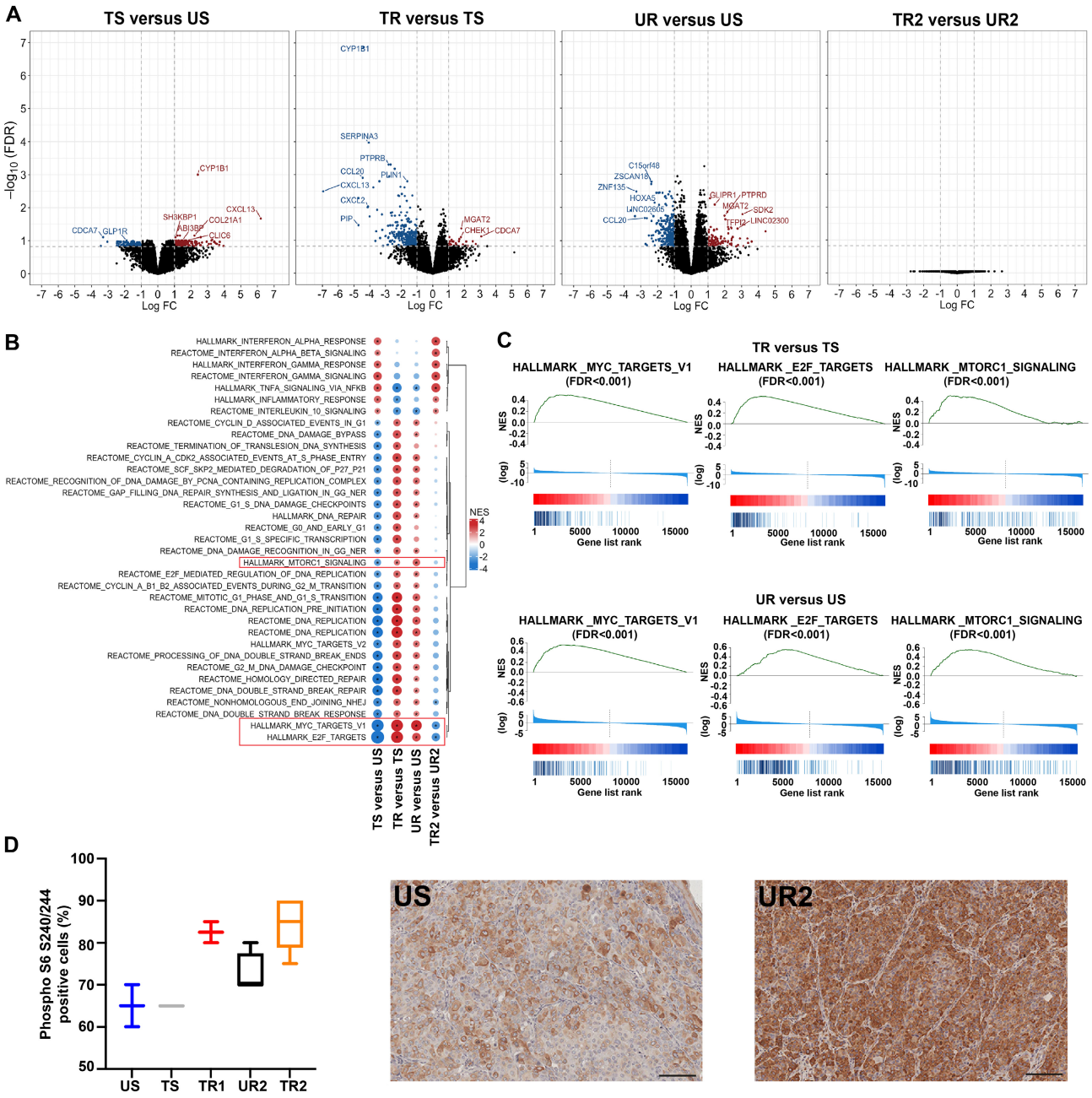

Figure 4. Palbociclib resistance is associated with upregulation of proliferation, DNA damage, and inflammatory response pathways, in tumor cells. (A) Volcano plots summarizing the results of differential analysis of human genes expressed by tumor cells. Group comparisons were: treated sensitive versus untreated sensitive (TS versus US), treated resistant versus treated sensitive (TR versus TS), untreated resistant versus untreated sensitive (UR versus US) and treated resistant versus untreated resistant second round (TR2 versus UR2). Significantly up- and down-regulated genes are indicated in red and blue, respectively. Selected top differentially expressed genes are highlighted. (B) Selected results of the Gene set Enrichment Analysis (GSEA) based on the differential analysis of human genes. Normalized enrichment scores (NES) and positive/negative associations are indicated by the circle size and color, respectively. Significant False Discovery Rate (FDR) is indicated by asterisk. Reported genesets are significant (FDR < 0.01% and |NES| > 2) in at least one comparison. Red boxes indicate gene sets also reported in the enrichment plots in (C). (C) Enrichment plots for the indicated pathways, in two group comparisons: treated resistant versus treated sensitive (TR versus TS), untreated resistant versus untreated sensitive (UR versus US). (D) Graph shows the quantification of S6 ribosomal protein phosphorylated at Ser240/244, measured by immunohistochemical staining of untreated and treated, sensitive and resistant tumors, as indicated (US, TS, TR1, UR2, TR2). On the right, two representative images from untreated sensitive (US, low pS6 staining) and untreated resistant (UR2, high pS6 staining) are shown. Scale bar, 100 μm. FC, Fold-Change.

biobank of 26 PDXs, derived from fresh specimens of surgically resected BC. These PDX models offer a more faithful representation of human BC, enabling a better understanding of tumor heterogeneity, and test potential therapeutic interventions with higher predictive accuracy [6–8]. Our engraftment rates were similar overall using different BC subtypes: 10% for luminal A, 18% for luminal B, 12% for HER2+, with the exception of TN (35%), already known to be much easier and quicker to engraft [27–29]. In our cohort, the engraftment rate showed no clear correlation with the sample origin (primary tumor, local recurrence or lymph

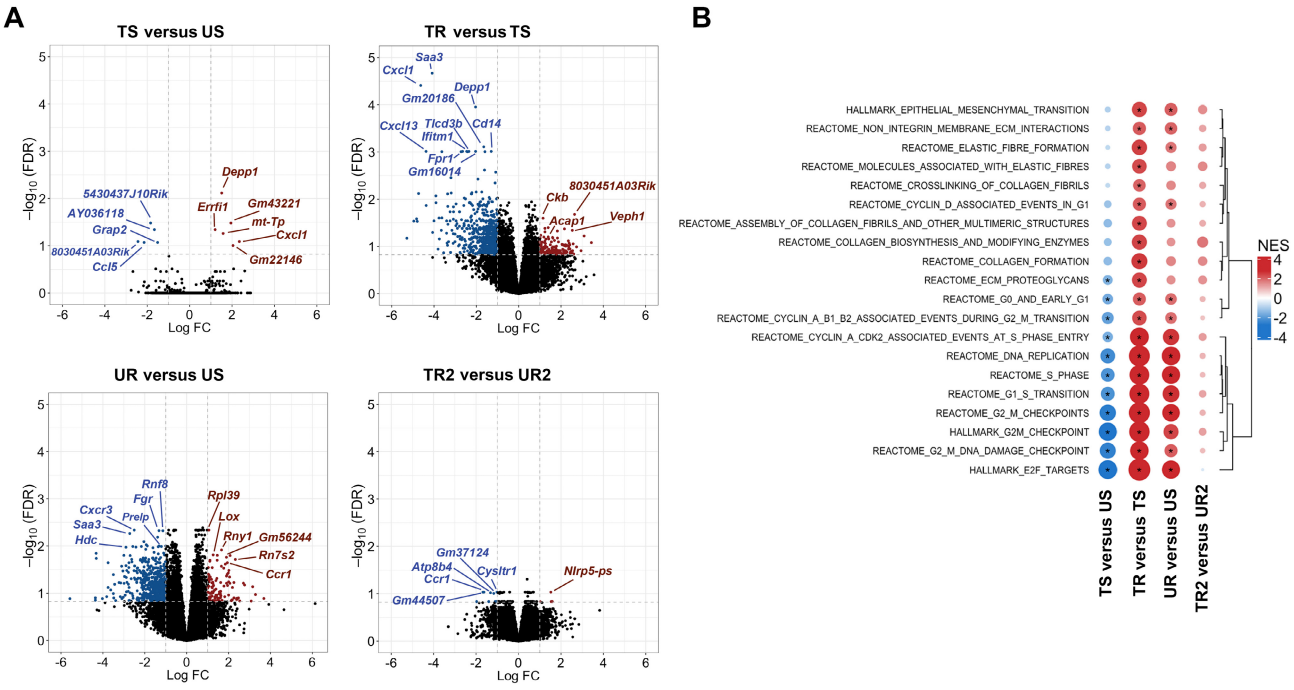

Figure 5. Palbociclib resistance is associated with stromal enrichment of extracellular matrix (ECM) remodeling and epithelial–mesenchymal transition (EMT) pathways. (A) Volcano plots summarize the results of differential analysis of mouse genes expressed by the tumor microenvironment. Group comparisons were: treated sensitive versus untreated sensitive (TS versus US), treated resistant versus treated sensitive (TR versus TS), untreated resistant versus untreated sensitive (UR versus US) and treated resistant versus untreated resistant second round (TR2 versus UR2). Significantly up- and down-regulated genes are indicated in red and blue, respectively. Selected top differentially expressed genes are highlighted. (B) Selected results of the Gene set Enrichment Analysis (GSEA) based on the differential analysis of mouse genes. Normalized enrichment scores (NES) and positive/negative associations are indicated by the circle size and color, respectively. Significant False Discovery Rate (FDR) is indicated by asterisk. Reported gene sets are significant (FDR < 0.01% and |NES| > 2) in at least one comparison. FC, Fold-Change.

node metastasis), patient age, or mutations in two most frequently mutated genes, *PIK3CA* and *TP53*. However, it did correlate with tumor grade and the capacity to grow under treatment. Specifically, tumors collected from patients who did not achieve PCR in the neoadjuvant setting displayed a higher intrinsic ability to survive and adapt to 'hostile' environments, such as the engraftment into the murine mammary gland.

Approximately 70% of all BCs express the hormone receptors (luminal BC, LBC). However, most models of LBC do not maintain the hormone receptor expression *in vivo*, making the understanding of the mechanisms underlying disease progression and drug response quite complicated. For this reason, we particularly focused on the generation and characterization of PDX from ER+, HER2− tumors, for which the availability of models is still scarce. Overall, ER positivity is considered an important favorable prognostic factor in BC, predictive of endocrine therapy sensitivity. However, more than 30% of patients with LBC eventually experience relapse in disease after endocrine therapies and patients with advanced or metastatic disease are often resistant *de novo*. In the advanced setting, patients with LBC are treated first line with endocrine therapy *plus* CDK4/6 inhibitors (CDK4/6i) [11,12]. However, resistance to CDK4/6i occurs very frequently and the discovery of successful approaches able to prevent or overcome resistance is still in progress [15]. Generation of drug resistant PDX models may represent a crucial step to investigate the mechanisms underlying resistance (both primary and secondary), since it may allow for its molecular and spatial characterization and for the testing of new ways to overcome it. To this aim, we generated PDX models of CDK4/6i sensitive and resistant LBC, both from *de novo* resistant tumors and from a sensitive one that acquired resistance following continuous treatment with the CDK4/6i palbociclib, which lasted over 6 months. We performed thorough transcriptomic characterization of the models with acquired resistance since they closely resemble the clinical situation of many patients with LBC, initially responding and eventually relapsing, under CDK4/6i treatment. Although having the limitation of an immunocompromised context, these PDXs have the great advantage of discerning the contribution of tumor cells (human side) from that of the tumor microenvironment (mouse side), here mainly constituted by cancer associated fibroblasts, the vascular system and extracellular matrix, simply by aligning data with the human or the murine genomes. Pathways necessary for the bypass of cell cycle blockade imposed by palbo, such as *MYC*, *E2F* and *MTORC1*, were greatly enriched in CDK4/6i resistant tumors, as expected [13–15]. It is interesting to note that, notwithstanding the immunocompromised context, tumor cells under palbo-treatment upregulated pathways that, in turn, stimulated the inflammatory and immune responses, especially in

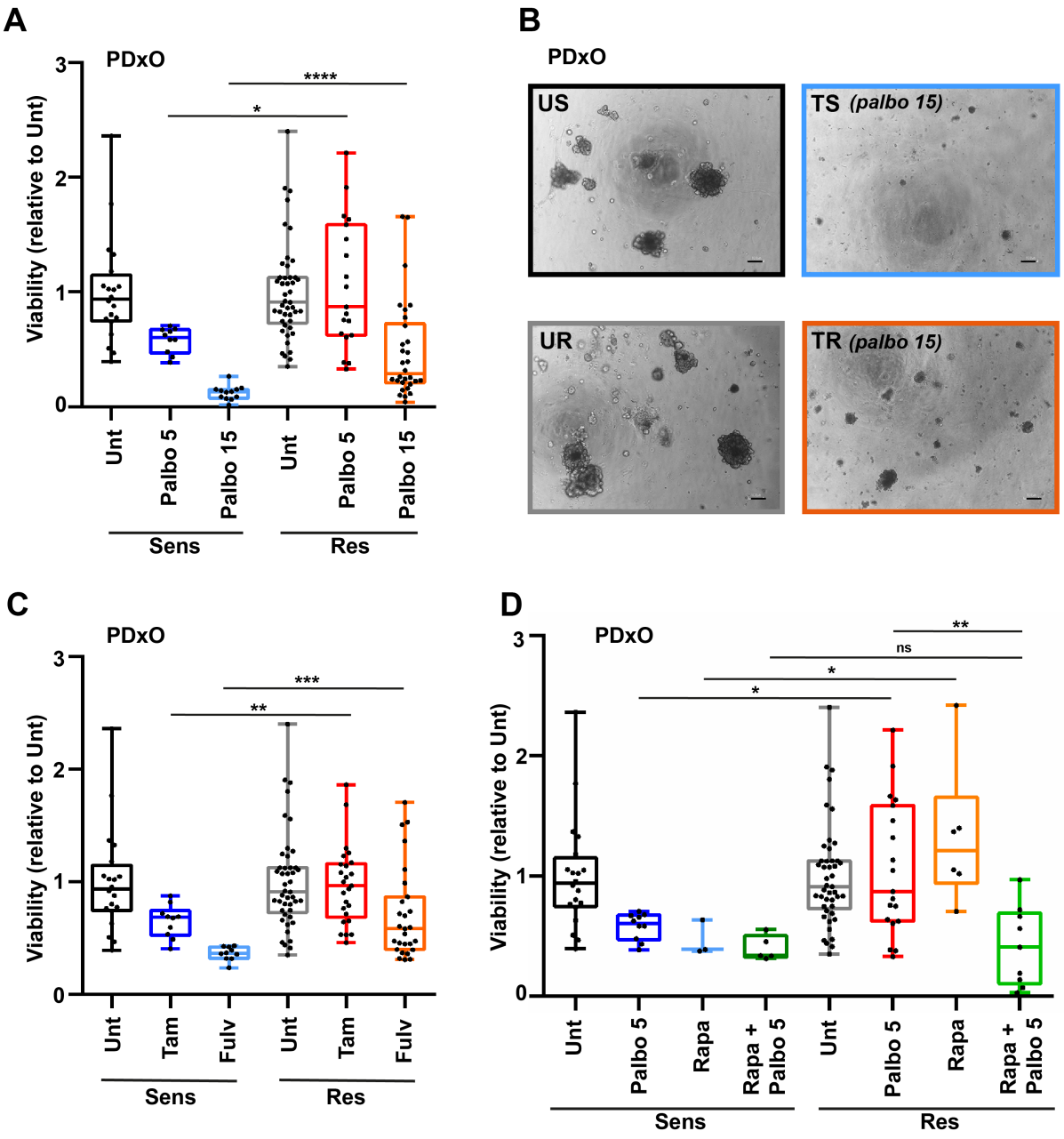

Figure 6. MTORC1 pathway inhibition reverts palbociclib resistance in PDxO models. (A) Graph reports the viability of organoids generated from PDX (PDxO) sensitive or resistant to palbociclib, as indicated, quantified using Cell Titer Glo reagent. PDxO were grown in complete medium and then treated with vehicle (Unt), palbociclib (Palbo) at 5 μM and 15 μM for 3 days. (B) Representative images of PDxO untreated (US and UR) or treated with palbociclib 15 μM (TS and TR). Scale bar, 100 μm. (C) Same as in (A) but treating PDxO with tamoxifen (Tam) 5 μM or fulvestrant (Fulv) 5 μM, as indicated. (D) Same as in (A) but treating PDxO with Palbo5 μM, the mTOR inhibitor rapamycin (Rapa) 0.5 μM, alone or in combination with Palbo 5 μM, as indicated. All treatment conditions (Unt, Palbo 5, Palbo 15, Tam, Fulv, Rapa, Rapa + Palbo, reported in A, C and D) were administered during the same experiments. For clarity, we have reported some of the treatments in different graphs. Specifically, the untreated and Palbo 5 μM conditions, shown in (A), are the same as also reported in (C) and (D), where they are used as controls. In all graphs, data were normalized to the untreated condition (Unt) and statistical significance was calculated using a Mann–Whitney test and expressed by p value <0.05. Box plots represent median, minimum and maximum values of the different experiments, performed in triplicate. Each dot corresponds to one individual experimental replicate. *$p < 0.05$; **$p < 0.01$; ***$p < 0.001$; ****$p < 0.0001$; ns, not significant.

CDK4/6i sensitive PDXs. This is in line with the well recognized immunomodulatory ability of CDK4/6i [35] and may indicate one further way that full resistance is achieved, that is, by attenuating the recruitment of immune cells to the tumor site. On the stromal side, the enrichment of pathways related to extracellular matrix remodeling and epithelial-mesenchymal transition in resistant tumors opens the way for intriguing avenues of investigation. It remains to be determined whether this transformation is a consequence or driver of resistance acquisition.

A known consequence of long-term use of palbo is that it stimulates the cells to enter into a state of senescence [36]. While this can overall be considered a positive effect of CDK4/6i, it can also elicit several

negative consequences. It is indeed plausible that senescent tumor cells might, especially in the long term, transform the tumor microenvironment, contributing, in turn, to the 'awaking' potential that senescent cancer cells maintain, eventually driving tumor regrowth, drug resistance and disease relapse in patients.

Intriguingly, the appearance of palbo-resistance is also associated with alteration in DNA-repair pathways. This finding suggests that these tumors may become vulnerable to DNA damaging agents and that combining CDK4/6i with chemotherapy or poly ADP ribose polymerase (PARP) inhibitors may represent a valid option in this setting, as we recently demonstrated in ovarian cancer [37].

Among numerous pathways, we focused our investigation on the MTORC1 pathway [31–33], since its inhibitors, such as everolimus, were FDA approved in the pre-CDK4/6 era to treat patients with advanced LBC [34]. Recently, MTORC1 has also been identified as an important mediator of luminal progenitors' aberrant function and dysregulation, in a *BRCA2*-mutated model, eventually leading to mammary transformation and ER+ tumorigenesis [38]. Also in that context, blocking MTORC1 substantially targeted a critical vulnerability and delayed breast tumorigenesis.

To assess MTORC1 involvement in palbociclib resistance, we employed a feasible yet patient-tumor feature-adherent approach using PDxOs. Our results proved that CDK4/6i resistance could be successfully overcome by MTORC1 inhibitors, paving the way to new therapeutic approaches for patients with LBC at high risk of developing recurrence. However, both the advancements in the understanding of cancer progression and the discovery of novel treatments rely on well characterized murine tumor models. Demonstrating efficacy in these models is essential for novel treatment strategies to progress to clinical testing. So, to increase the clinical relevance of our findings, we certainly intend to extend our experimentation to the appropriate PDX models from our biobank. As exemplified by our characterization of CDK4/6i resistance, the set-up and conduction of 'xenotrials' in PDX provides molecular insights into each therapeutic arm, within the same tumor. While impossible in humans, this approach holds significant potential in enhancing our understanding of drug response and resistance pathways.

Taken together, considering the substantial number of patients with luminal BC experiencing recurrence, the frequent emergence of drug resistance, and the increasing number of young patients, it is imperative to generate appropriate models to investigate resistance mechanisms and identify more effective treatment approaches. By establishing this biobank of BC specimens and PDX, we have generated living tools for future basic, translational and preclinical research.

Acknowledgements

We are grateful to the patients who consented to donating their samples. We would also like to thank all present and past members of the SCICC laboratory for their valuable contribution; all members of the Molecular Oncology Unit for critical discussion of the data; all members of the Pathology Unit and CRO biobank for their excellent technical support. This work was supported by the Associazione Italiana per la Ricerca sul Cancro (AIRC) to B Belletti (AIRC IG#20061); by Ministero della Salute to B Belletti (RF-2021-12371961) and I Segatto (GR-2021-12373937); by CRO Intramural Research Seed Grant (5X1000_2016_MdS) to I Segatto; by CRO Intramural Research Grant 5 ‰ MdS (BraCaCuRe) to B Belletti; by Alleanza Contro il Cancro (ACC) to B Belletti (RCR-2022-23682287); by Ministero dell'Università (ARS01_00568) to G Baldassarre; and by Ricerca Corrente Linea 1 core grant of Ministero della Salute. The funders had no role in the design of the study; in the collection, analyses, or interpretation of data; in the writing of the manuscript; or in the decision to publish these results. Open access funding provided by BIBLIOSAN.

Author contributions statement

BB and IS designed, supervised and conducted experiments, acquired and analyzed the data, and wrote the manuscript. BB, IS and MCM generated PDX and PDxO. MCM, NC, LM, AF, ADA, GDG, GM, SDA, CG and FR conducted experiments and acquired the data. GLRV and TP provided pathological and immunohistochemical analyses. MD, RB and MC provided support for the analyses of DNA- and RNA-seq data. LG, FP and SM provided clinical data. GB analyzed and critically discussed the data and contributed to the manuscript writing. All authors discussed the results, reviewed and approved the final manuscript.

Data availability statement

RNA sequencing data are deposited using the Annotare tool of EMBL-EBI (https://www.ebi.ac.uk/fg/annotare/) (fgsubs #740862). The data that support the findings of this study are openly available in Annotare/ArrayExpress EMBL-EBI at https://www.ebi.ac.uk/fg/annotare, reference number 740862.

References

1. Gennari A, André F, Barrios CH, *et al*. ESMO clinical practice guideline for the diagnosis, staging and treatment of patients with metastatic breast cancer. *Ann Oncol* 2021; **32:** 1475–1495.
2. Loibl S, André F, Bachelot T, *et al*. Early breast cancer: ESMO clinical practice guideline for diagnosis, treatment and follow-up. *Ann Oncol* 2024; **35:** 159–182.
3. Perou CM, Sørlie T, Eisen MB, *et al*. Molecular portraits of human breast tumours. *Nature* 2000; **406:** 747–752.

4. Sørlie T, Perou CM, Tibshirani R, *et al*. Gene expression patterns of breast carcinomas distinguish tumor subclasses with clinical implications. *Proc Natl Acad Sci U S A* 2001; **98:** 10869–10874.
5. Schettini F, Brasó-Maristany F, Kuderer NM, *et al*. A perspective on the development and lack of interchangeability of the breast cancer intrinsic subtypes. *NPJ Breast Cancer* 2022; **8:** 85.
6. Guillen KP, Fujita M, Butterfield AJ, *et al*. A human breast cancer-derived xenograft and organoid platform for drug discovery and precision oncology. *Nat Cancer* 2022; **3:** 232–250.
7. Hutten SJ, De Bruijn R, Lutz C, *et al*. A living biobank of patient-derived ductal carcinoma in situ mouse-intraductal xenografts identifies risk factors for invasive progression. *Cancer Cell* 2023; **41:** 986–1002.e9.
8. Dobrolecki LE, Airhart SD, Alferez DG, *et al*. Patient-derived xenograft (PDX) models in basic and translational breast cancer research. *Cancer Metastasis Rev* 2016; **35:** 547–573.
9. Howlader N, Altekruse SF, Li CI, *et al*. US incidence of breast cancer subtypes defined by joint hormone receptor and HER2 status. *J Natl Cancer Inst* 2014; **106:** dju055.
10. Burstein HJ. Systemic therapy for estrogen receptor–positive, HER2-negative breast cancer. *N Engl J Med* 2020; **383:** 2557–2570.
11. Spring LM, Wander SA, Andre F, *et al*. Cyclin-dependent kinase 4 and 6 inhibitors for hormone receptor-positive breast cancer: past, present, and future. *Lancet* 2020; **395:** 817–827.
12. Morrison L, Loibl S, Turner NC. The CDK4/6 inhibitor revolution – a game-changing era for breast cancer treatment. *Nat Rev Clin Oncol* 2023; **21:** 89–105.
13. Xu X, Pan X, Wang T, *et al*. Intrinsic and acquired resistance to CDK4/6 inhibitors and potential overcoming strategies. *Acta Pharmacol Sin* 2021; **42:** 171–178.
14. Papadimitriou MC, Pazaiti A, Iliakopoulos K, *et al*. Resistance to CDK4/6 inhibition: mechanisms and strategies to overcome a therapeutic problem in the treatment of hormone receptor-positive metastatic breast cancer. *Biochim Biophys Acta Mol Cell Res* 2022; **1869:** 119346.
15. Lloyd MR, Spring LM, Bardia A, *et al*. Mechanisms of resistance to CDK4/6 blockade in advanced hormone receptor–positive, HER2-negative breast cancer and emerging therapeutic opportunities. *Clin Cancer Res* 2022; **28:** 821–830.
16. DeRose YS, Gligorich KM, Wang G, *et al*. Patient-derived models of human breast cancer: protocols for in vitro and in vivo applications in tumor biology and translational medicine. *Curr Protoc Pharmacol* 2013; **60**: 14.23–14.23.43.
17. Wolff AC, Hammond MEH, Allison KH, *et al*. Human epidermal growth factor receptor 2 testing in breast cancer: American Society of Clinical Oncology/College of American Pathologists Clinical Practice Guideline Focused Update. *J Clin Oncol* 2018; **36**: 2105–2122.
18. World Health Organization. *World Health Statistics 2019: Monitoring Health for the SDGs: Sustainable Development Goals*. World Health Organization: Geneva, 2019.
19. Sachs N, De Ligt J, Kopper O, *et al*. A living biobank of breast cancer organoids captures disease heterogeneity. *Cell* 2018; **172:** 373–386.e10.
20. Citron F, Armenia J, Franchin G, *et al*. An integrated approach identifies mediators of local recurrence in head and neck squamous carcinoma. *Clin Cancer Res* 2017; **23:** 3769–3780.
21. Viotto D, Russo F, Anania I, *et al*. CDKN1B mutation and copy number variation are associated with tumor aggressiveness in luminal breast cancer. *J Pathol* 2021; **253:** 234–245.
22. Gerratana L, Basile D, Franzoni A, *et al*. Plasma-based longitudinal evaluation of ESR1 epigenetic status in hormone receptor-positive HER2-negative metastatic breast cancer. *Front Oncol* 2020; **10:** 550185.
23. Segatto I, Berton S, Sonego M, *et al*. p70S6 kinase mediates breast cancer cell survival in response to surgical wound fluid stimulation. *Mol Oncol* 2014; **8:** 766–780.
24. Segatto I, Zompit MDM, Citron F, *et al*. Stathmin is required for normal mouse mammary gland development and Δ16HER2-driven tumorigenesis. *Cancer Res* 2019; **79:** 397–409.
25. Callari M, Batra AS, Batra RN, *et al*. Computational approach to discriminate human and mouse sequences in patient-derived tumour xenografts. *BMC Genomics* 2018; **19:** 19.
26. Dobin A, Davis CA, Schlesinger F, *et al*. STAR: ultrafast universal RNA-seq aligner. *Bioinformatics* 2013; **29:** 15–21.
27. Park HS, Lee JD, Kim JY, *et al*. Establishment of chemosensitivity tests in triple-negative and BRCA-mutated breast cancer patient-derived xenograft models. *PLoS One* 2019; **14:** e0225082.
28. Landuzzi L, Palladini A, Ceccarelli C, *et al*. Early stability and late random tumor progression of a HER2-positive primary breast cancer patient-derived xenograft. *Sci Rep* 2021; **11:** 1563.
29. Vaillant F, Merino D, Lee L, *et al*. Targeting BCL-2 with the BH3 mimetic ABT-199 in estrogen receptor-positive breast cancer. *Cancer Cell* 2013; **24:** 120–129.
30. Kabos P, Finlay-Schultz J, Li C, *et al*. Patient-derived luminal breast cancer xenografts retain hormone receptor heterogeneity and help define unique estrogen-dependent gene signatures. *Breast Cancer Res Treat* 2012; **135:** 415–432.
31. Herrera-Abreu MT, Palafox M, Asghar U, *et al*. Early adaptation and acquired resistance to CDK4/6 inhibition in estrogen receptor–positive breast cancer. *Cancer Res* 2016; **76:** 2301–2313.
32. Costa C, Wang Y, Ly A, *et al*. PTEN loss mediates clinical cross-resistance to CDK4/6 and PI3Kα inhibitors in breast cancer. *Cancer Discov* 2020; **10:** 72–85.
33. Rodriguez MJ, Perrone MC, Riggio M, *et al*. Targeting mTOR to overcome resistance to hormone and CDK4/6 inhibitors in ER-positive breast cancer models. *Sci Rep* 2023; **13:** 2710.
34. Baselga J, Campone M, Piccart M, *et al*. Everolimus in postmenopausal hormone-receptor-positive advanced breast cancer. *N Engl J Med* 2012; **366:** 520–529.
35. Goel S, DeCristo MJ, Watt AC, *et al*. CDK4/6 inhibition triggers anti-tumour immunity. *Nature* 2017; **548:** 471–475.
36. González-Gualda E, Baker AG, Fruk L, *et al*. A guide to assessing cellular senescence *in vitro* and *in vivo*. *FEBS J* 2021; **288:** 56–80.
37. Dall'Acqua A, Sonego M, Pellizzari I, *et al*. CDK6 protects epithelial ovarian cancer from platinum-induced death via FOXO3 regulation. *EMBO Mol Med* 2017; **9:** 1415–1433.
38. Joyce R, Pascual R, Heitink L, *et al*. Identification of aberrant luminal progenitors and mTORC1 as a potential breast cancer prevention target in BRCA2 mutation carriers. *Nat Cell Biol* 2024; **26:** 138–152.

SUPPLEMENTARY MATERIAL ONLINE

Supplementary materials and methods

Figure S1. Patient-derived xenografts (PDXs) maintain the histopathological features of the original human breast cancer

Figure S2. Stable PDX#18 and PDX#28 retain the expression of biomarkers of the originating human tumors

Figure S3. Patient-derived xenografts (PDXs) maintain the morphological features of the originating human tumors.

Figure S4. Acquisition of palbociclib resistance alters gene expression

Figure S5. Acquisition of palbociclib resistance is associated with gene set alteration, in both human and murine components of patient-derived xenografts (PDXs)

Table S1. Clinico-pathological features of all patients with breast cancer for whom patient-derived xenografts (PDXs) were attempted ($n = 151$)

Table S2. Summary of individual tumor information of the 26 established PDX lines, together with their matched tumors

Table S3. Summary of somatic mutations on *PIK3CA*/*AKT1* and *TP53* genes in the 26 established patient-derived xenograft (PDX) lines and in their matched tumors